Green Fluorescent Protein Variants as Ratiometric Dual Emission pH Sensors. 1. Structural Characterization and Preliminary Application†

George T. Hanson,‡ Tim B. McAnaney,§ Eun Sun Park,§ Marla E. P. Rendell,‡ Daniel K. Yarbrough,‡ Shaoyou Chu,|| Lixuan Xi,|| Steven G. Boxer,§ Marshall H. Montrose,|| and S. James Remington*,‡

Departments of Chemistry and Physics and Institute of Molecular Biology, University of Oregon, Eugene, Oregon 97403-1229, Department of Chemistry, Stanford University, Stanford, California 94305-5080, and Department of Cellular and Integrative Physiology, Indiana University, Indianapolis, Indiana 46202-5120

Received August 9, 2002; Revised Manuscript Received October 1, 2002

ABSTRACT: Novel dual emission, pH-sensitive variants of the green fluorescent protein (GFP) have been constructed and are suitable for ratiometric emission measurements in vivo. This new class of GFPs, termed deGPFs, results from substitution of wild-type residue 65 with threonine and residues 148 and/or 203 with cysteine. deGFPs display pK_a values ranging from 6.8 to 8.0 and emission that switches from a green form (λ_{max} ∼515 nm) to a blue form (λ_{max} ∼460 nm) with acidifying pH. In this report we analyze in most detail the deGFP1 variant (S65T/H148G/T203C, pK_a ∼8.0) and the deGFP4 variant (S65T/C48S/H148C/T203C, pK_a ∼7.3). In the following paper [McAnaney, T. B., Park, E. S., Hanson, G. T., Remington, S. J., and Boxer, S. G. (2002) *Biochemistry 41*, 15489−15494], data obtained by ultrafast fluorescence upconversion spectroscopy can be described by a kinetic model that includes an excited-state proton-transfer pathway at high pH but not at low pH. Crystal structure analyses of deGFP1 at high-pH and low-pH conformations were performed to elucidate the basis for the dual emission characteristics. At low pH the structure does not contain a hydrogen bond network that would support rapid transfer of a proton from the excited state of the neutral chromophore to a suitable acceptor; hence blue emission is observed. At high pH, backbone rearrangements induced by changes in the associated hydrogen bond network permit excited-state proton transfer from the excited state of the neutral chromophore to the bulk solvent via Ser147 and bound water molecules, resulting in green emission from the anionic chromophore. Comparative analysis suggests that the basis for dual emission is elimination of the wild-type proton-transfer network by the S65T substitution, a general reduction in hydrogen-bonding opportunities, and a concomitant increase in the hydrophobic nature of the chromophore environment resulting from the cysteine substitutions. We evaluated the suitability of the deGFP4 variant for intracellular pH measurements in mammalian cells by transient expression in PS120 fibroblasts. The responses of deGFP4 and a commercially available pH-sensitive dye, SNARF-1, to changes in pH were compared in the same cells. Results show that the dynamic range of the emission ratio change is comparable between the two pH sensors over the range examined. Two-photon excitation was found to elicit a better deGFP4 fluorescent signal above cellular autofluorescence when compared to conventional confocal microscopy. Given their favorable optical characteristics, suitable pK_a's for the physiological pH range, and suitability for ratiometric measurements, dual emission GFPs should make excellent probes for studying pH in vivo.

The *Aequorea victoria* green fluorescent protein (GFP)[1] has become one of the most popular fluorescent indicators for protein localization and gene expression in cell and molecular biology research (see reviews, refs *1*−*3*). This popularity stems largely from the fact that GFP is genetically encoded, making it tractable for use in subcellular compartments and ideal for fusion to proteins of interest, tasks that are difficult to accomplish with small molecule fluorescent indicators.

While these applications are spectacularly successful, the potential for GFP variants as biosensors in cells is conceivably much greater. Recent studies have demonstrated the possibility of utilizing GFP variants to report intracellular pH (*4*−*8*), Ca^{2+} concentration (*9*−*13*), halide ion concentration (*14*, *15*), protein−protein interactions (*16*), and tyrosine kinase activity (*17*) and possibly to indicate redox status in living cells (*18*; G. T. Hanson and S. J. Remington, manuscript in preparation). However, a major drawback for use in vivo of many of the proposed biosensors is that the analyte concentration often affects only the intensity of fluorescence. Therefore, it is difficult to determine whether observed changes in fluorescence are due to changes in analyte concentration or indicator GFP concentration, and this is further complicated by inevitable photobleaching. Consequently, an independent means of measuring indicator GFP concentration is required in most cellular applications.

† This work was supported in part by NIH Grants R01-GM42618-11 to S.J.R., RO1-DK42457 to M.H.M., and GM-27738 to S.G.B.

* To whom correspondence and reprint requests should be addressed. Tel: (541) 346-5190. Fax: (541) 346-5870. E-mail: jim@uoxray.uoregon.edu.

‡ University of Oregon.

§ Stanford University.

|| Indiana University.

[1] Abbreviations: ESPT, excited-state proton transfer; rms, root mean square; GFP, green fluorescent protein; deGFP, dual emission GFP.

10.1021/bi026609p CCC: $22.00
Published on Web 12/07/2002

Ratiometric probes, which have multiple excitation or emission maxima that show opposing changes in fluorescence excitation or emission in response to changes in analyte concentration, are potentially much more useful. Ratiometric measurements can reduce or eliminate distortions of data caused by photobleaching, indicator concentration, variable cell thickness, illumination stability, excitation path length, and nonuniform indicator distribution within cells or between groups of cells (*19*).

Wild-type GFP can in principle provide a basis on which to construct indicators suitable for either emission or excitation ratiometric measurements. The excitation spectrum of wild type is characterized by two major absorption bands (UV band A and visible band B) attributed to an internal ground-state equilibrium between the neutral and anionic forms of the chromophore, respectively (*1*). The excited state of the neutral chromophore would be expected to fluoresce in the blue and the anionic chromophore in the green; however, in wild type the blue fluorescence is very weak (*20*), and predominantly green fluorescence is observed upon excitation at either absorption maximum. This is because fast internal proton transfer from the excited state of the neutral chromophore produces the anion and results in green fluorescence (*21*, *22*). Detailed atomic models for the proton relay network responsible for the two-wavelength excitation behavior of wild-type GFP have been proposed (*23*−*25*). Many GFP variants have been reported that alter the excitation characteristics of the green fluorescence (*1*, *26*), but few [other than substitution of the chromophore component Tyr66 (*27*)] have been described that have large consequences for emission wavelengths. It is reasonable to suppose that given modifications to the proton-transfer networks in GFP, variants could be found that display strong blue fluorescence, for example, by slowing down ESPT from the excited state of the neutral chromophore.

Although in wild-type GFP the ratio of the two absorption bands does not depend strongly on pH or ionic strength in the physiological range (*28*), pH-sensitive GFP variants that are ratiometric by excitation have been reported (*7*, *8*, *29*, *30*). These variants retain the two absorption bands characteristic of wild type, but the ratio of the neutral and anionic populations depends strongly on pH. While such characteristics are very promising, two-wavelength excitation measurements are not universally adaptable to techniques such as flow cytometry and laser scanning microscopy, where the availability of required laser lines and/or the speed of wavelength switching can be restrictive. Even with modern instruments that utilize acoustic optical tunable filters to switch wavelengths within milliseconds, the time lag during data collection can limit experimental resolution of dynamic ratio changes in living cells. Furthermore, intensity fluctuations in the excitation sources can introduce significant errors in the method (*19*). The limitations of two-wavelength excitation measurements are most pronounced in two-photon fluorescence microscopy. The pulsed lasers currently available for two-photon excitation output a single wavelength at a given time and require manual adjustment to alter excitation wavelengths.

Fluorescent indicators that are ratiometric by emission are therefore very desirable. To date, the only individual fluorescent protein displaying dual emission characteristics is the "fluorescent timer" (*31*). This indicator, which is a variant of the red fluorescent protein drFP583 (dsRed; *32*), uses the green emitting intermediate that is transiently formed during the multistep maturation process, which slowly converts into the red emitting product. A fusion of two fluorescent proteins (UV-GFP and YFP) has also been recently described as a ratiometric pH indicator with a pK_a of ~6.8 (*33*).

In this report, we describe the spectral and structural properties of a novel class of individual fluorescent proteins (deGFPs) that display dual emission and provide improved ratiometric pH indicators. These indicators respond to pH changes by opposing changes in blue and green emission and have biologically relevant pK_a's. Here we evaluate the spectroscopic and structural properties of two of the most promising deGFP variants and confirm the utility of one variant (deGFP4) as an intracellular pH indicator in mammalian cells using confocal and two-photon microscopy.

MATERIALS AND METHODS

Mutagenesis and Protein Preparation. Mutagenesis was carried out on a histidine-tagged version of the S65T variant of GFP in the plasmid pRSET$_B$. Mutations were introduced via the QuikChange site-directed mutagenesis kit (Stratagene, La Jolla, CA), following the manufacturer's protocol. DNA sequencing of the entire GFP coding sequence verified all mutations. Mutant protein was expressed in *Escherichia coli*, strain JM109(DE3), by use of the pRSET$_B$ expression system with an N-terminal His$_6$ tag. The cells were resuspended in 50 mM HEPES, pH 7.9, 300 mM NaCl, and 10% glycerol and sonicated for 7 min. Cell lysate was centrifuged, and the supernatant was applied to a column of Ni-NTA agarose resin (Qiagen, Hilden, Germany). The N-terminal histidine tag was cleaved with 2% (w/w) γ-chymotrypsin overnight at room temperature. Debris was removed, samples were concentrated by filtration (Centricon 10, Amicon), and buffer was exchanged with PD-10 Sephadex columns (Amersham Pharmacia) into 20 mM HEPES, pH 7.9.

pH Titrations. The pH dependence of absorbance and fluorescence emission was determined using 20−200 μg mL^{-1} deGFP in 75 mM buffer and 140 mM NaCl. Buffers appropriate for the desired pH were chosen from MES, HEPES, or CHES, and the final pH was adjusted by HCl or NaOH addition. The absorbance was then recorded between 250 and 550 nm on a Shimadzu 2101 spectrophotometer. Molar extinction coefficients were determined using the theoretical ϵ_{280} [19890 M^{-1} cm^{-1} (*34*)] for GFP S65T, and protein concentrations were determined using two different methods, BCA (Pierce) and the Bradford assay using bovine serum albumin as a standard (Bio-Rad).

Fluorescence measurements were performed on Hitachi F4500 and Perkin-Elmer LS55B fluorescence spectrophotometers at a protein concentration of 20−100 μg mL^{-1} in the same buffers used for absorbance measurements. Apparent pK_a values were determined by plotting the emission intensities of the two major absorption (400 and 505 nm) and two major emission peaks (460 and 515 nm) as a function of pH. The data were fit independently (Kaleidagraph, Abelbeck Software) to titration curves of the form:

$$I(\mathrm{pH}) = C + D/(1 + 10^{\mathrm{p}K_a - \mathrm{pH}})$$

where D is the dynamic range and C is an offset. The

chromophore is never fully anionic in any of these variants at pH <10 (see Results). Therefore, the extinction coefficient (ϵ_{505}) for the anionic (B) form of the chromophore was estimated from the extinction coefficient (ϵ_{400}) of the neutral (A) form at pH 5.5 and the derivative of the theoretical titration curve

$$dI/d(pH) = \ln(10)\, D \times 10^{pK_a - pH}/(1 + 10^{pK_a - pH})^2$$

for each of the two absorption bands, each independently fitted as a function of pH. The ratio of the extinction coefficients $\epsilon_{505}/\epsilon_{400}$ is equal to $|D_{505}/D_{400}|$. A simpler approach, which in practice is less sensitive to end point errors, is to evaluate the slope *M* of a linear fit to intensity versus pH near the midpoint of the titration curve. In this case the ratio of the extinction coefficients $\epsilon_{505}/\epsilon_{400}$ is $|M_{505}/M_{400}|$. The absorbance spectra were corrected for small pipetting errors by scaling curves to have identical summed absorbance in the range 270−280 nm, which substantially improved the consistency of the results.

Fluorescence Quantum Yields. The quantum yields of emission for excitation close to each absorbance maximum were determined. Solutions (∼100 mg/mL) of each protein were prepared in 100 mM citrate, pH 5.5−6.0, or 100 mM Tris, pH 9.0, as required in order to maximize the neutral or anionic forms of the chromophore, respectively. At pH <5.5, some evidence for protein instability was noted. Standards were prepared using 9-aminoacridine dissolved in water ($\lambda_{max,abs}$ = 400 nm) or fluorescein dissolved in 0.1 N NaOH ($\lambda_{max,abs}$ = 496 nm) such that the absorbance of the standard was equal to the absorbance of the protein at the chosen wavelength. Total emission for excitation at 400 or 496 nm was measured for each dye and protein sample using a Perkin-Elmer LS-55B fluorescence spectrophotometer. The emission spectra were corrected for detector response using the manufacturer-supplied correction curves and integrated using the supplied software (FLWinlab). Quantum yields for the protein samples were calculated from the total emission ratios using accepted values for the dye standards [Φ_F = 0.98 for 9-aminoacridine and Φ_F = 0.92 for fluorescein (*35*)]. As a check the quantum yield for GFP S65T (λ_{ex} = 490 nm) was determined and found to be 0.71, which is in good agreement with values quoted in the literature (*1*).

Crystallization. deGFP1 protein, S65T/H148G/T203C, was concentrated to approximately 48 mg mL^{-1} in 20 mM HEPES (pH 7.9) and subjected to 0.2 μm filtration. Rod-shaped crystals grew at room temperature in 1−2 days by hanging drop vapor diffusion against 100 mM citrate−NaOH (pH 4.5), 100 mM ammonium acetate, 14% poly(ethylene glycol) 1550 (final measured pH 5.5) for the low-pH crystals and 50 mM Tris (pH 9.0), 100 mM $MgCl_2$, 22% poly-(ethylene glycol) 4000 for the high-pH crystals. Drops contained 4 μL of protein solution and 4 μL of well solution. For diffraction data collection at 100 K, low-pH crystals were exchanged over 3 days into a solution of 100 mM citrate−NaOH (pH 4.5), 100 mM ammonium acetate, and 40% poly-(ethylene glycol) 1550 (final measured pH 5.5). The high-pH crystals were exchanged into 50 mM Tris (pH 9.0), 100 mM $MgCl_2$, 22% poly(ethylene glycol) 4000, and 40% ethylene glycol.

X-ray Data Collection and Refinement. X-ray diffraction data were collected from a single flash-frozen crystal at 100 K for each pH using an Raxis-IV image plate mounted on a Rigaku RUH3 rotating anode generator equipped with mirrors for the low-pH data set and using a Mar 345 detector at the Stanford Synchrotron Radiation Laboratory beamline 7-1 for the high-pH data set. Data sets were indexed and reduced with MOSFLM, and intensities were scaled with SCALA (*36*). The GFP S65T coordinate file (PDB code: 1EMA) was used as the initial phasing model. Positional refinement was carried out using the data to 4.0, 3.0, 2.5, 2.1, 1.8, and finally to the limit of resolution, using the program TNT (*37*). After each increase in resolution the electron density maps ($2F_o - F_c$ and $F_o - F_c$) were analyzed using the program O (*38*). *B*-Factor refinement was performed using the default TNT *B*-factor correlation library. The *B*-factor correlation values for the chromophore atoms were derived from histidine and phenylalanine residues. The atomic coordinates and structure factors have been deposited in the Protein Data Bank (http://www.rcsb.org/, access codes 1JBY and 1JBZ).

Mammalian Cell Expression and Imaging. The deGFP4 coding sequence was amplified by PCR from the $pRSET_B$ vector, using primers that included *Eco*RI and *Not*I restriction sites that allowed swapping of deGFP4 for the conventional EGFP in the pEGFP-N1 mammalian expression vector (Clontech, Palo Alto, CA). The PS120 fibroblast cell line was seeded onto glass coverslips and transfected with the plasmid (Fugene 6, Roche). Two days after transfection, coverslips were mounted in a microscope chamber, allowing continuous superfusion of cells with physiologic medium (130 mM NaCl, 5 mM KCl, 2 mM $CaCl_2$, 1 mM $MgSO_4$, 1 mM $NaPO_4$, 25 mM mannose, and 20 mM HEPES, pH 7.4). Cells were imaged on a Zeiss LSM 510 confocal microscope after being loaded with 2 mM SNARF-1 AM (Molecular Probes, Eugene, OR). During imaging, 25 mM NH_4Cl solution (added to the physiologic medium above) was transiently superfused over cells to induce cellular pH changes. All images were collected simultaneously during excitation at 364 nm (2−5 mW from an Ar laser) and 543 nm (0.2−0.6 mW from an HeNe laser) for deGFP4 and SNARF-1, respectively, while monitoring emission at 385−470 and 475−525 nm for deGFP4 and 560−615 and 625−655 nm for SNARF-1. Data were analyzed using Metamorph software (Universal Imaging, Downingtown, PA). Cellular autofluorescence was estimated as the average fluorescence either from the same cells prior to dye loading (SNARF-1 values) or from nontransfected cells in the same field of view (deGFP4 values). After subtraction of cellular autofluorescence values, ratio images were calculated for both SNARF (625−655/560−615 nm) and deGFP4 (475−525/385−470 nm) as described previously (*39*). Average ratio values were calculated from individual cells.

Transfected cells were also imaged in a Zeiss LSM510 NLO two-photon microscope. For imaging, cells transfected with deGFP4 were excited with 810 nm light from a femtosecond-pulsed titanium−sapphire laser, with the emission simultaneously recorded at 435−485 and 490−685 nm. For measuring two-photon excitation or emission spectra, droplets of purified deGFP4 (100 μg/mL in the physiologic saline solution) were measured on the NLO microscope stage. For emission spectra, two-photon fluorescence was excited at 810 nm, collected via a fiber optic, and routed to an imaging spectrograph (Triax 320 with back-thinned, liquid

nitrogen cooled CCD; YJ Horiba Instruments) for simultaneous collection of the 430−670 nm emission. For excitation spectra, the Ti:S excitation wavelength was varied from 750 to 850 nm while keeping the average power entering the NLO scan head fixed at 56 mW. The imaging spectrograph was used to collect fluorescence in response to changes in excitation wavelength so that intensity of specific emission wavelengths could be quantified.

RESULTS

Construction of Dual Emission GFPs. Dual emission GFP variants were discovered in the course of experiments in which different types of amino acids were introduced at positions Thr203 and His148, each of which are known to profoundly influence the absorption and emission characteristics of GFP (*26*, *29*). In a remarkable experiment, substitution of Thr203 with His was recently shown to result in a weakly fluorescent GFP that is photoactivatable (*40*). All variants described in this study (Table 1) contain the S65T substitution (*39*), which is critical for pH-dependent dual emission behavior (see Discussion). In general, the amino acid at position 65 is a strong determinant of the pH sensitivity of GFP variants. Unlike wild-type GFP, most variants at position 65 exhibit large changes in fluorescence in response to changes in pH, the prototype being S65T with a pK_a of about 6.1. We have previously reported that the dual point mutation S65T/H148D is not only pH-sensitive but ratiometric by excitation as it retains the dual excitation maxima of wild type (*29*).

We replaced Thr203 and His148 individually and in tandem with cysteine, which introduces potentially charged, polarizable SH groups into the immediate vicinity of the chromophore hydroxyl. In two instances, the naturally occurring cysteine 48, which is on the surface of the protein far from the chromophore, was replaced with serine to prevent possible formation of undesirable inter- or intramolecular cross-links. The C48S substitution is phenotypically neutral (data not shown). Finally, the dual substitution S65T/H148G, which has only a hydrogen atom for a side chain at position 148, is reported as a control.

The cysteine-containing mutants all displayed blue fluorescence in acidified solution and exhibited dual emission. The color changes are visually dramatic either in solution or in the crystalline material. We selected two variants (S65T/H148G/T203C, deGFP1, and C48S/S65T/H148C/T203C, deGFP4) for further characterization. The deGFP1 variant was constructed on a background of S65T/H148G, which was expected from other experiments (*14*) to have a relatively high chromophore pK_a, while deGFP4 has a pK_a that is closer to neutrality.

Absorption and Emission Spectroscopy. In Table 2, the pH-dependent spectroscopic properties of five of the resulting variants are summarized, four of which show dual emission behavior. Each deGFP mutant displays two absorption and two emission bands. The pK_a values were independently determined from the two absorption and two emission bands and averaged. They are 8.02, 7.29, 6.86, and 7.37 for deGFPs 1−4, respectively (Table 2). The extinction coefficient (ϵ_{400}) of the neutral chromophore and the estimated extinction coefficient ratio ($\epsilon_{505}/\epsilon_{400}$) do not vary greatly between the different deGFPs. Averaging the measurements yields the final estimates of $\epsilon_{400} = 26000$ and $\epsilon_{505} = 47000$ M^{-1} cm^{-1} for the neutral and anionic chromophore, respectively.

Table 1: Sequence Changes and Nomenclature for deGFP Variants[a]

name	amino acid substitutions
deGFP1	S65T/H148G/T203C
deGFP2	S65T/C48S/H148C
deGFP3	S65T/T203C
deGFP4	S65T/C48S/H148C/T203C

[a] All variants contain the ubiquitous Q80R substitution which evidently arose during the original cloning (*1*).

Table 2: Spectroscopic Properties of deGFP Variants[a]

	H148G	deGFP1	deGFP2	deGFP3	deGFP4
$\lambda_{abs,A}$[b] (nm)	397	400	398	396	400
ϵ_A[c] (M^{-1} cm^{-1})	25000	28700	21700	26700	26900
$\lambda_{abs,B}$[b] (nm)	492	504	496	508	509
ϵ_B/ϵ_A[d]		1.91	1.76	1.72	1.89
ϵ_B[c] (M^{-1} cm^{-1})	40500	54800	38200	45900	50800
$\lambda_{em,A}$[e] (nm)	weak	465513	461515	460512	461515
$\lambda_{em,B}$[e] (nm)	512	516	517	518	518
Φ_{AL}[f]		0.046	0.12	0.12	0.08
Φ_{AH}[f]		0.16	0.34	0.19	0.15
Φ_B[f]	0.43	0.49	0.55	0.57	0.27
pK_a[g]	7.0	8.02(8)	7.25(5)	6.86(6)	7.37(9)
em ratio[h] (%)		12	7	13	20

[a] Extinction coefficients and quantum yield values were measured for absorption bands A (UV) and B (visible) at pH 5.5−6.0 and 9.0 as discussed in Materials and Methods. [b] λ_{abs} are the peaks in the absorbance spectrum (nm) for absorption band A and band B. [c] ϵ_A and ϵ_B are the molar extinction coefficient for absorbance at 400 nm (band A) and 505 nm (band B). ϵ_B was calculated from ϵ_A and the ratio of ϵ_B/ϵ_A as discussed in Materials and Methods. For H148G, ϵ_B was determined experimentally from the absorbance spectrum. [d] The ratio of the extinction coefficients of band B to band A, experimentally determined from the derivatives of the pH titration curves as discussed in Materials and Methods. [e] λ_{em} is the peak(s) in the emission spectrum corresponding to excitation at the wavelength maximum of absorbance band A and band B, respectively. [f] Φ is the fluorescence quantum yield. Values are given for emission with excitation at 400 nm at pH 5.5−6.0 (Φ_{AL}) and at pH 9.0 (Φ_{AH}) and for emission from the anionic chromophore at pH 9.0 with excitation at 496 nm (Φ_B). [g] pK_a is the apparent midpoint in the pH titration of the chromophore; average values were determined from independent titrations of the two absorbance bands at 400 and 505 nm and two emission bands at 460 and 515 nm. The number in parentheses is the observed standard deviation in the last digit of the averaged value. For H148G, the pK_a was determined from the pH dependence of band B absorbance. [h] The ratio of maximum emission intensity at 460 nm to maximum emission intensity at 515 nm.

The absorbance spectra of deGFP1 and deGFP4 as a function of pH are shown in panels A and B of Figure 1. At pH <10, both proteins exhibit a strong absorption at 400 nm characteristic of the neutral form of the chromophore. At high pH, the chromophore is partially converted into the anionic form which absorbs at >500 nm, but in no case is this process complete before the protein begins to unfold, at pH >10 (data not shown). The spectra have sharp isosbestic points characteristic of only two interconverting species. The changes in absorbance with pH can be accurately fit to a titration curve appropriate for a single titrating species, which results in an apparent pK_a of 8.02 for deGFP1 and 7.37 for deGFP4, the double cysteine mutant. In the latter case, only a small percentage of the chromophore is in the anionic form at any biologically relevant pH.

When excited at 400 nm (band A) at pH <7.0, the steady-state emission spectra of deGFP1 (Figure 1C) and deGFP4

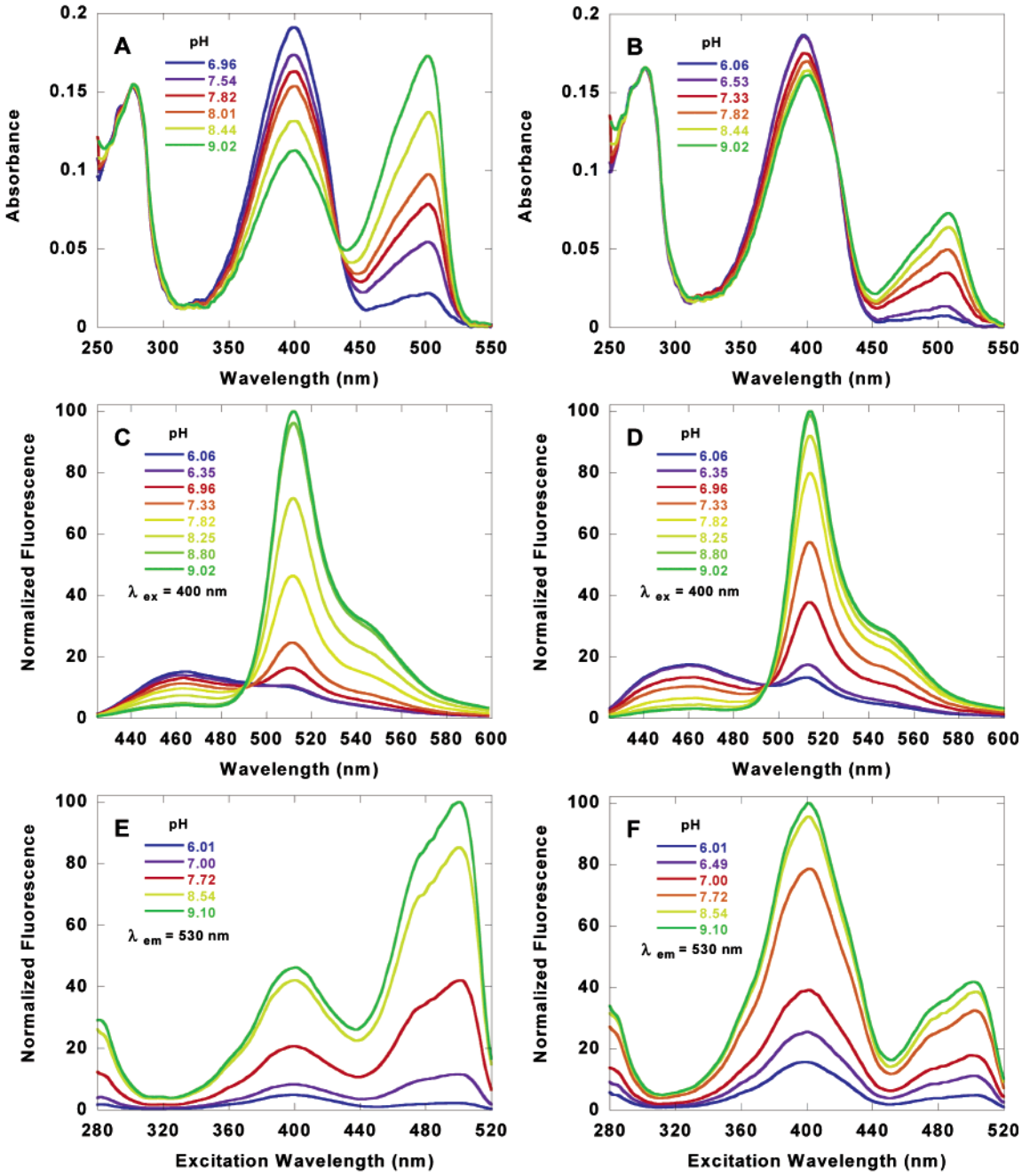

FIGURE 1: Absorbance (A, B), fluorescence emission for excitation at 400 nm (C, D), and fluorescence excitation (E, F) spectra with detection at 530 nm plotted as a function of pH. Normalization was performed by setting the maximum observed intensity to 100 and scaling the other curves in each plot by the same factor. deGFP1 (A, C, E); deGFP4 (B, D, F).

(Figure 1D) display a very broad blue peak with a maximum at about 460 nm, extending to beyond 550 nm. At higher pH, a narrower green emission peak centered at about 515 nm (Figure 1C,D) is observed. Band B corresponding to the anionic chromophore can be excited directly at 480−500 nm, in which case only green emission can be observed. Hence, we define *dual emission* as emission at ~460 and ~515 nm, with relative intensities depending on pH, for excitation of the neutral chromophore at 400 nm. Compared to deGFP1, the deGFP4 variant has a more favorable pK_a and a 77% increase in the relative intensity of the blue emission peak (460 nm) relative to the green emission peak (515 nm).

Excitation spectra of deGFP1 (Figure 1E) and deGFP4 (Figure 1F), for fluorescence emission at 530 nm, are intriguing. Both proteins are efficiently excited at 280 nm, suggesting energy transfer from aromatic residues to the chromophore and/or direct excitation of the chromophore. As the pH increases, the intensity of the 530 nm emission increases for all excitation wavelengths. When fluorescence emission is detected at 460 nm for excitation at 280−450 nm, the spectra have similar peaks but the pH dependence of the emission intensity is the opposite (data not shown). As with the absorption spectra, the pH dependence of each emission maximum can be very accurately modeled by a theoretical curve corresponding to a single titrating species.

The blue fluorescence from these mutants is of low intensity because of low quantum yields (Table 2). We surmise that this is due to the reduced number of hydrogen bonds to the chromophore, discussed in a later section, resulting in a flexible environment with greater freedom for

Table 3: Data Collection and Refinement Statistics for deGFP1 at Low and High pH

	pH 5.5	pH 9.0
data collection		
total observations	83420	120478
unique reflections	18906	34536
cell dimensions (*a*, *b*, *c*, Å)	50.95, 62.24, 67.20	51.2, 62.37, 68.97
resolution (Å)	19.5−1.80	19.9−1.50
highest resolution shell (Å)	1.90−1.80	1.58−1.50
completeness[a] (%)	93.0 (87.2)	96.2 (93.6)
multiplicity[a]	4.4 (4.3)	3.5 (3.3)
av I/σ[a]	6.4 (2.7)	9.3 (2.3)
R_{merge}[a,b]	0.062 (0.273)	0.045 (0.319)
refinement		
spacegroup	$P2_12_12_1$	$P2_12_12_1$
no. of protein atoms	1743	1760
no. of solvent atoms	114	202
R-factor[c]	0.194	0.177
av *B*-factors (Å^2)	40.8	24.4
protein atoms	40.4	22.5
solvent	45.8	39.9
deviations from ideality		
bond lengths (Å)	0.012	0.013
bond angles (deg)	2.1	2.2
B-factor correlation (Å^2)	5.3	4.0

[a] Values in parentheses give statistics for the highest resolution shell. [b] $R_{merge} = \sum|I - \langle I\rangle|/\sum\langle I\rangle$, where I is the observed intensity and $\langle I\rangle$ is the average of intensity obtained from multiple observations of symmetry-related reflections. [c] *R*-factor $= \sum||F_o| - |F_c||/\sum|F_o|$, where F_o and F_c are the observed and calculated structure factors, respectively.

energy dissipation by fast competing processes such as vibration or conformational change. This interpretation is consistent with the broad nature of the blue emission band, which implies numerous opportunities for energy dissipation prior to light emission. Presumably, it would be possible to optimize the quantum yield of blue fluorescence by directed evolution.

Structural Analysis of Low- and High-pH deGFP1 Crystals. To elucidate the structural basis for the dual emission behavior of these variants, crystallization trials were initiated. The deGFP1 variant produced useful crystals, essentially isomorphous to S65T GFP, at both low and high pH. The crystal structures were determined by molecular replacement and refined at 1.8 and 1.5 Å resolution, respectively. There is one molecule of deGFP1 in the asymmetric unit of each crystal, and the final models have satisfactory geometry and crystallographic *R*-factors (Table 3).

Comparison of the high- and low-pH structures of deGFP1 with those of S65T GFP at high and low pH (*29*) reveals that the β-barrel motif characteristic of GFP is maintained at both pH values (Figure 2A). In both models the Sγ of Cys203, which is very clearly defined by the electron density maps, occupies the position normally occupied by the Cγ2 of Thr203. This leaves the hydrogen bond donor/acceptor position normally occupied by the Thr203 Oγ1 (*29*) vacant. Removal of the imidazole chain of His148 by substitution with glycine results in minor translations of the backbone and does not create a cavity permitting solvent access to the chomophore. Glu222, which has been proposed to be the ultimate proton acceptor upon excited-state proton transfer (*23*, *24*), adopts the conformation seen in the S65T structure (*41*) at both high and low pH. In this conformation, the carboxylate is required by the hydrogen bond configuration

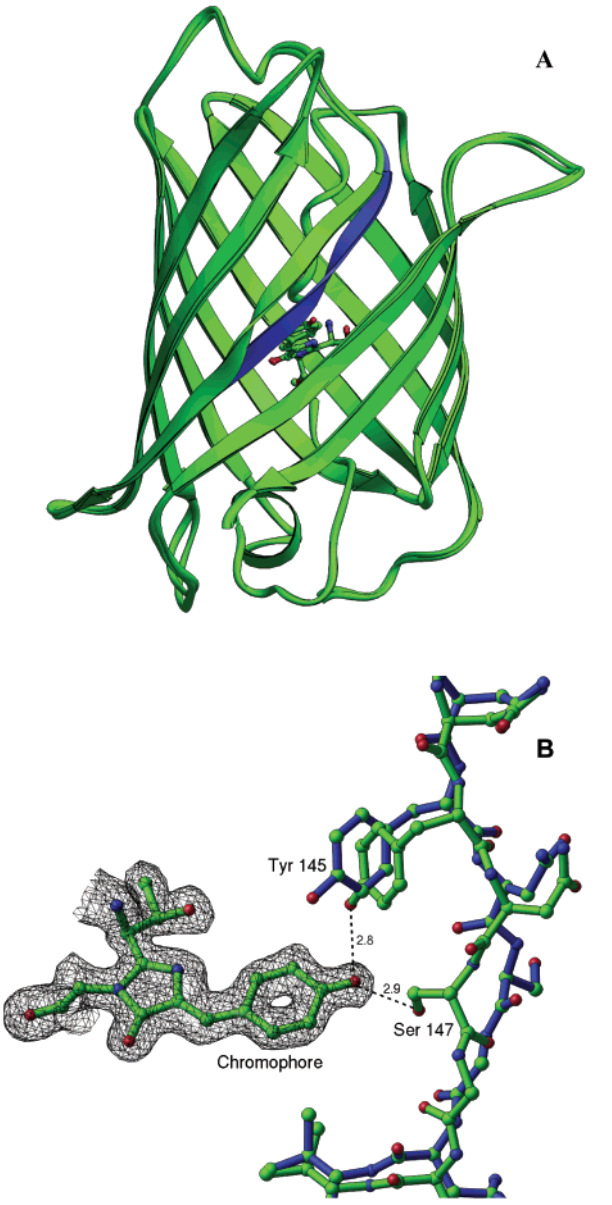

FIGURE 2: (A) Schematic drawing of the superimposed backbones of deGFP1 at high and low pH showing the displacement of the strand containing residues 143−150. The backbone ribbon for residues 143−150 of the low-pH structure is drawn in blue. The chromophore is represented by a ball-and-stick figure. This figure was prepared using MOLSCRIPT (*45*). (B) A portion of the $2F_o - F_c$ electron density map at 1.5 Å resolution for deGFP1 at high pH. The map is contoured at a level of 1 SD of the electron density. The refined atomic model of the chromophore is shown superimposed on the density map. Adjacent to the chromophore, residues 143−149 are shown in a ball-and-stick representation. Strands: blue, low pH; green, high pH. The hydrogen bonds from the hydroxyls of residues 145 and 147 to the chromophore at high pH are shown as dotted lines and have the indicated lengths in angstroms.

to be protonated and cannot be a proton acceptor in ESPT. Consequently, in deGFP1, at neither pH structure does there appear to be a proton relay network that resembles that found in wild-type GFP. For reference, the complete arrangement of hydrogen bonds near the chromophore in the pH 5.5 and 9.0 crystals is illustrated schematically in Figure 3.

At low pH, except for very minor rearrangements due to replacement of His148 with Gly, the S65T (Protein Data Bank designation 1EMA) and deGFP1 structures are es-

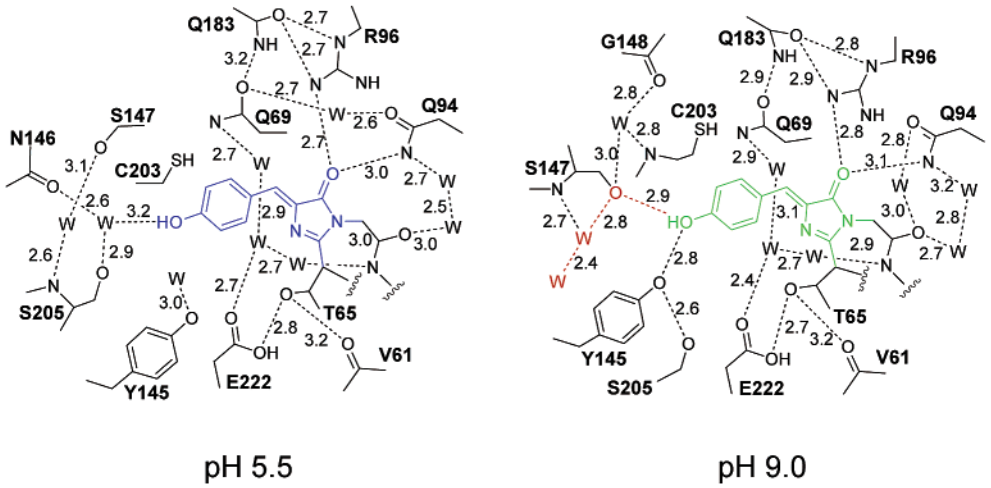

FIGURE 3: Schematic drawing of the hydrogen bond network associated with the chromophore of deGFP1 at low pH and high pH. The dashed lines indicate hydrogen bonds with the indicated lengths in angstroms. The red dashed lines and W's indicate water molecules proposed to provide a transfer of a proton in the excited state to bulk solvent. Although the high-pH chromophore structure is shown as protonated (green), its protonation state in the crystal cannot be determined from the electron density map. The spectroscopy reveals that, in solution, the chromophore is at least partially in the anionic state at pH 9.0.

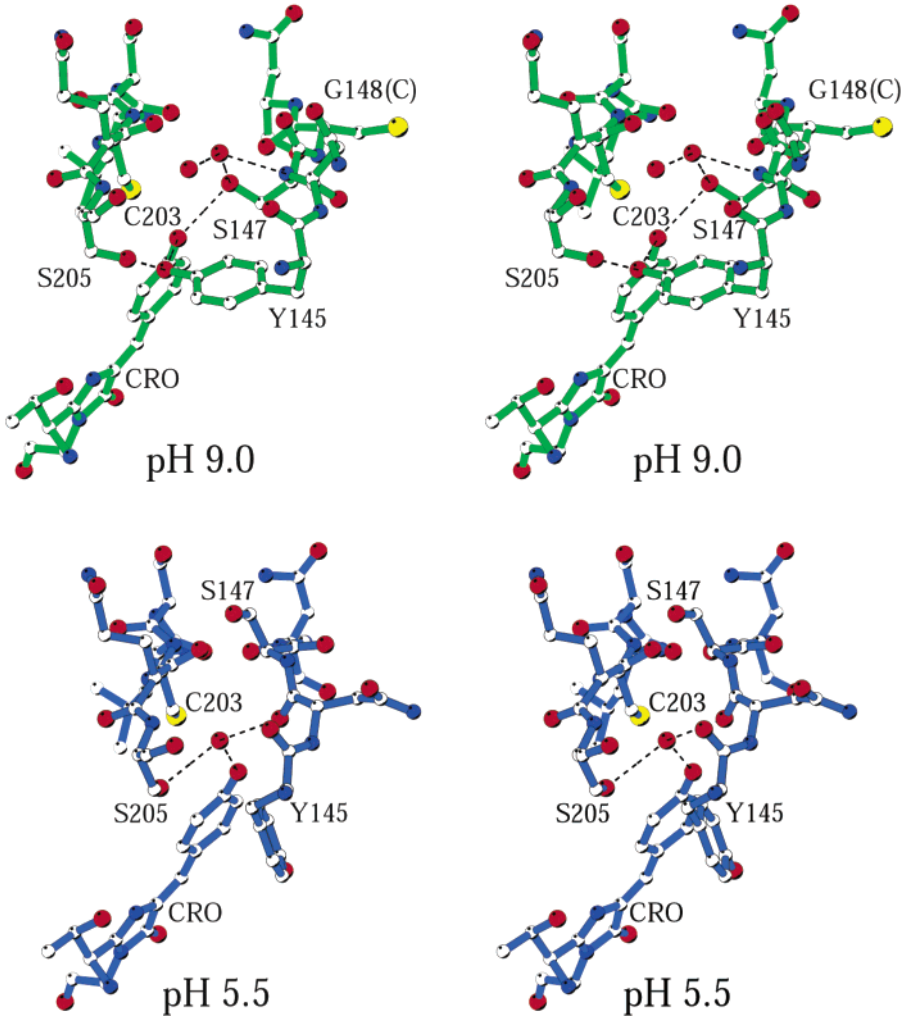

FIGURE 4: Stereoview of portions of the atomic models for the low-pH and high-pH deGFP1 crystal structure. Oxygen is colored red, nitrogen blue, and sulfur yellow. For comparison, in the top part of the illustration, the deGFP4 substitution of Cys for Gly148 is illustrated as a hypothetical model. No short contacts with the model-built side chain to other parts of the protein are observed, suggesting that the deGFP4 structure could adopt essentially the same conformation seen with deGFP1.

sentially superimposable with deviations at the α-carbon positions of 0.33 Å rms, which is within the error of the structure determinations. Tyr145 and Ser147 avoid interaction with the chromophore hydroxyl, which we presume to

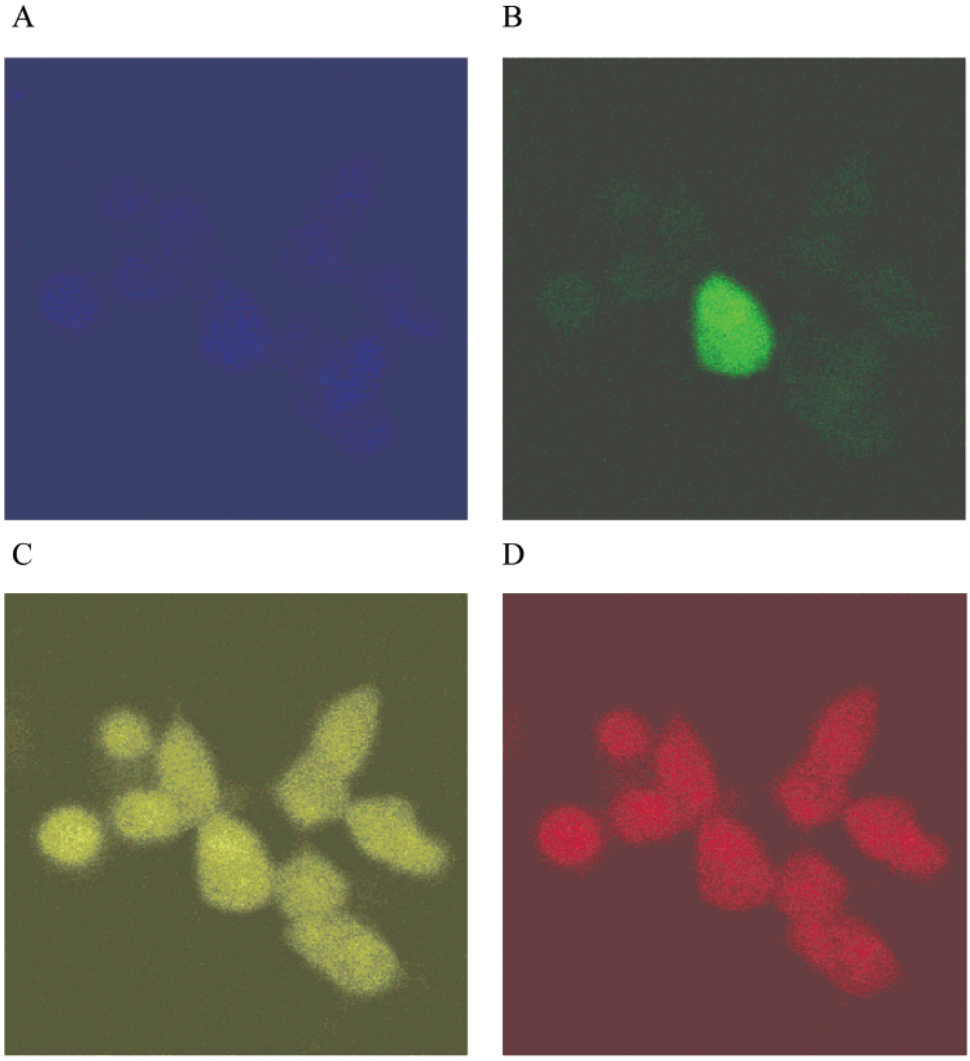

FIGURE 5: Images of PS120 cells transiently transfected with deGFP4 and loaded with SNARF-1. Live cells were imaged by confocal microscopy. Emission wavelengths for deGFP4 were 385−470 nm (A) and 475−525 nm (B) in response to 364 nm excitation. For SNARF-1, emission wavelengths were 560−615 nm (C) and 625−655 nm (D) in response to 543 nm excitation. Cellular autofluorescence occludes much of the 385−470 nm fluorescence of the deGFP4; however, 364 nm excitation is not optimal for this probe (see text).

be protonated (Figure 4, bottom). The hydroxyls of Tyr145 and Ser147 are positioned 4.0 and 5.8 Å away from the chromophore hydroxyl, respectively.

At pH 9.0, the rms deviation of α-carbon positions increases to 0.44 Å for the deGFP1 model compared to the S65T structure (1EMA, pH 8.1), largely because β-strand residues 143−150 adopt a conformation not seen in any other GFP structure. Atoms in residues 147−149 are displaced by up to 4 Å relative to their position at low pH (Figure 2). Furthermore, the side chains adopt substantially different orientations. The backbone motion places Tyr145 and Ser147 in position to form hydrogen bonds with the phenolic end of the chromophore, which we presume to be at least partially deprotonated at pH 9.0. At low pH the side chain of Ser147 faces the bulk solvent; however, at high pH, Ser147 flips to the interior of the protein, becomes inaccessible to bulk solvent, and forms hydrogen bonds with the chromophore hydroxyl and a bound water molecule (Figure 4, top).

In summary, comparison of the two structures reveals changes in the hydrogen bond configuration to the chromophore phenolic oxygen and that main and side chain atoms are closer to the chromophore at high pH. In particular, deGFP1 residues 143−150 undergo a remarkable rearrangement in response to changes in pH (Figure 2). The backbone flexibility at positions 147 and 148 is clearly essential for this rearrangement (Figure 4), as the peptide planes undergo substantial reorientation. The reduction in size of the side chain at position 148 and replacement of the branched Thr203 with cysteine appear to permit the main chain to adopt this new conformation. The region adjacent to residue 148 is not involved in crystal contacts, indicating the observed strand motion is not a consequence of the crystallization conditions.

DISCUSSION AND APPLICATION

pH-Dependent Conformational Change. Inspection of the model for the chromophore environment in the high- and low-pH deGFP1 crystals (shown schematically in Figure 3) permits one to draw some conclusions about the associated hydrogen bond networks. It is important to note that, at 1.5 Å resolution, hydrogen atoms cannot be directly visualized, but their positions can often be inferred from chemical and geometric considerations. For example, in structures containing the S65T mutation, proton locations may be assigned unambiguously in the vicinity of Glu222, and the conclusion can be drawn that Glu222 must be uncharged (*24*, *41*). In

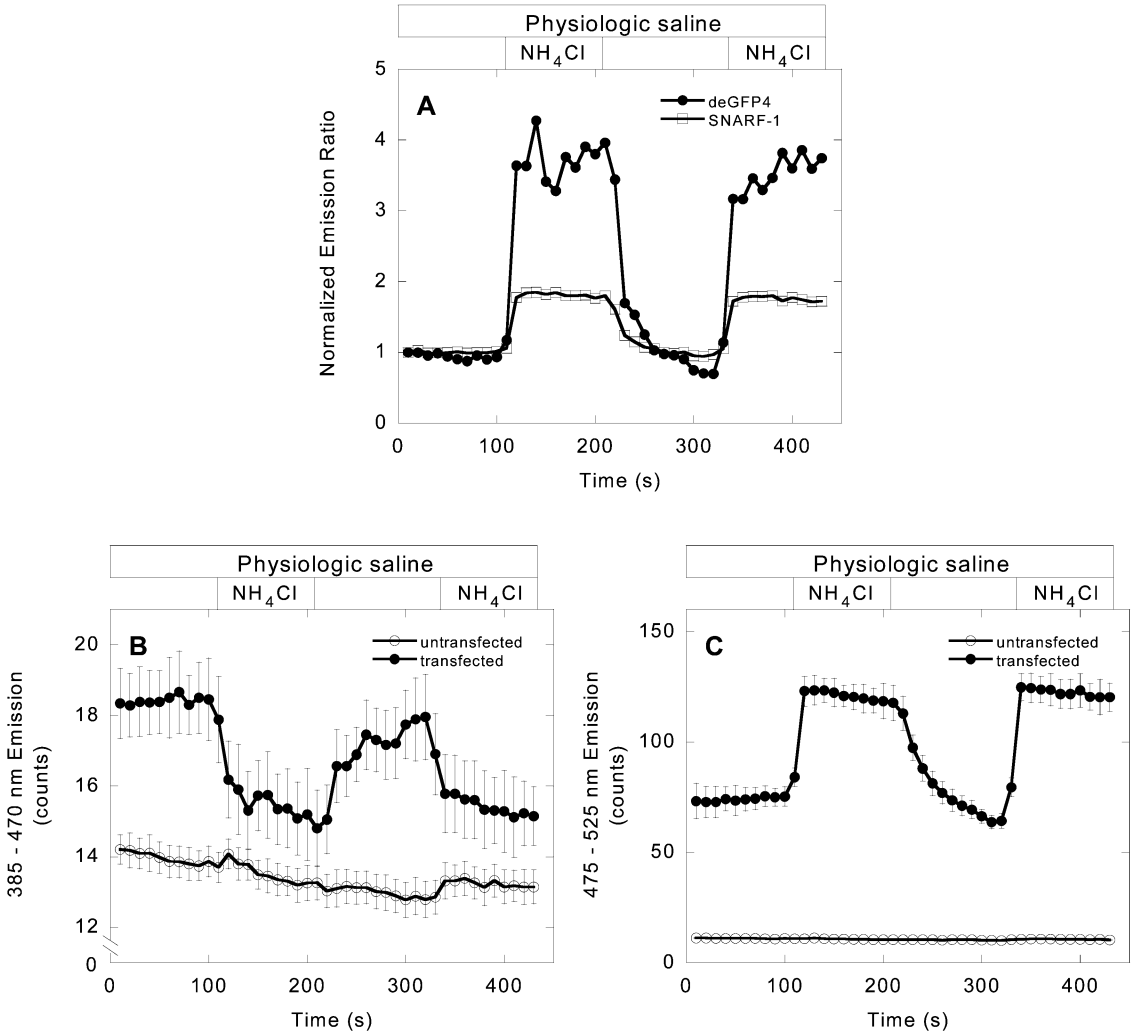

FIGURE 6: Time course of pH changes in PS120 cells, as monitored by SNARF-1 and deGFP4 using confocal microscopy. Cells were exposed to 25 mM NH_4Cl at the indicated times. (A) Emission ratio values were separately calculated for SNARF-1 (open circles) and deGFP4 (triangles) fluorescence in the same cells, as described in Materials and Methods. Ratio values for each indicator were then normalized to the ratio values observed in the cells at the start of the experiment. (B) To confirm that the low 385−470 nm fluorescence in deGFP4-expressing cells was pH-sensitive, total cellular 385−470 nm fluorescence was compared between 3 transfected cells (identified by 475−525 nm fluorescence; diamonds) and 12 surrounding nontransfected cells in the same field of view (open circles). Only the deGFP4-expressing cells demonstrate pH-sensitive fluorescence at 385−470 nm. (C) A similar analysis of total cellular 475−525 nm fluorescence shows that transfected cells have much greater 475−525 nm fluorescence than untransfected cells and demonstrates opposing responses to pH change compared to the 385−470 nm wavelength range.

deGFP1 there is a clear difference in the number and type of hydrogen bonds associated with the chromophore phenolic oxygen at high and low pH (Figure 3) with the presumption being that the chromophore is anionic at pH 9 and neutral at pH 5.5. The chromophore is the only ionizable group in the immediate vicinity, so the simplest explanation for the conformational differences observed for residues 143−150 is that they are driven by the changes in the hydrogen bond network associated with changes in the chromophore ionization state. The internalization of Ser147 at high pH can be rationalized by the energetically favorable formation of a hydrogen bond with the anionic chromophore hydroxyl.

These simple considerations are unfortunately difficult to reconcile with the spectroscopic observations. The spectroscopic response of each mutant has a well-defined pK_a which differs from mutant to mutant but corresponds to a theoretical model with two interconverting species. We assume that the spectroscopic signal is in response to and faithfully reflects the conformational differences observed in the crystal structures. However, from the spectral data, a large fraction of the chromophore population in all deGFPs is in the neutral state at pH <10. In the case of deGFP1, from the extinction coefficients (Table 2) and the absorption spectrum at pH 9.0 (Figure 1A) the ratio of the neutral to anionic populations in solution is 65:35. With deGFP4, the ratio of the neutral to anionic form is estimated to be 75:25 at pH 9.0.

If this ratio of protonation states holds in the crystal, one would expect mixed protonation states in the crystal at pH 9.0, possibly resulting in structural heterogeneity. However, neither the electron density maps (Figure 2B) nor the atomic *B*-factors provide any evidence for such heterogeneity. In both crystals, ($F_o - F_c$) difference electron density maps show no significant features near the chromophore (data not shown), so the single structural state modeled must account for at least 90% of the crystal contents. At pH 5.5, the average vibrational parameter (*B*-factor) is 38.8 Å^2 for all main chain atoms and 35.5 Å^2 for the 145−150 segment. At pH 9.0, the average *B*-factor is 23.0 Å^2 for all main chain

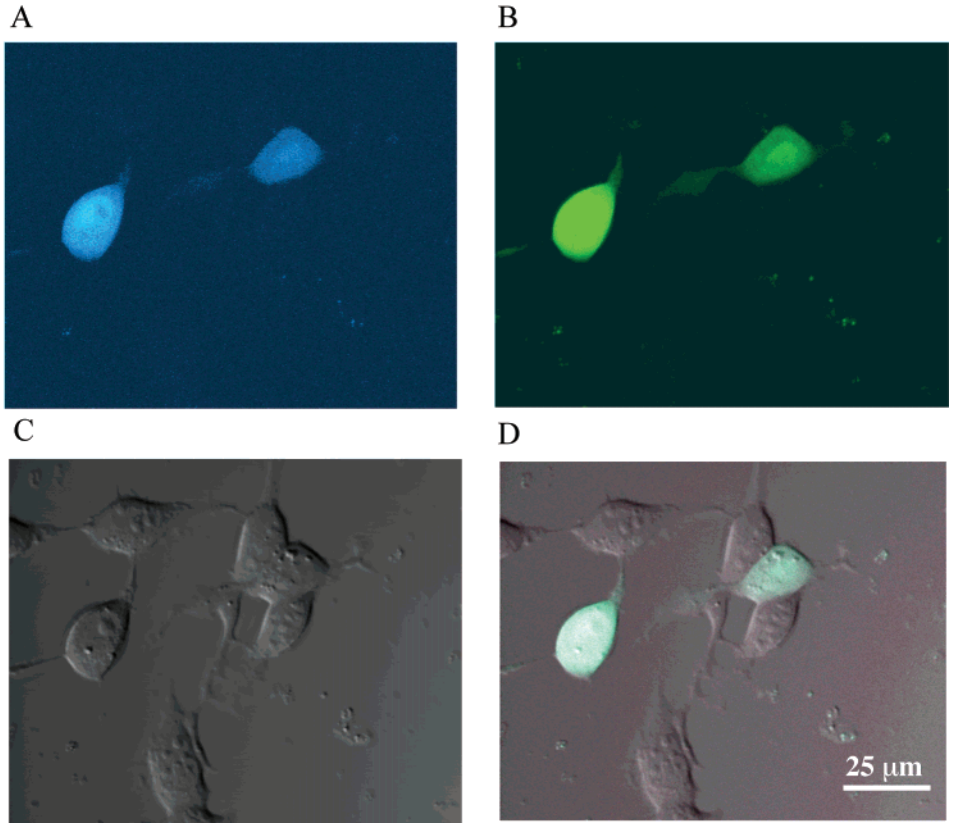

FIGURE 7: Two-photon microscopy images of PS120 cells transiently transfected with deGFP4. Emission wavelengths for visualization of deGFP4 were 435−485 nm (A) and 490−685 nm (B), in response to two-photon excitation at 810 nm. A transmitted light image (C) showing all cells, along with an overlay (D) of panels A−C, is shown.

atoms and 26.9 Å^2 for the 145−150 segment. Thus even if the pH 9.0 crystal is assumed to be heterogeneous with respect to chromophore protonation states (but predominantly neutral), the protein chain configuration reflects the hydrogen bond arrangement to the anionic chromophore. The protein thus seems to respond by chain rearrangement to the *average* protonation state of the chromophore in a highly cooperative fashion. In other words, the presence of only a small population of the anionic species at high pH appears to be sufficient to push the equilibrium for the chain reorganization to completion. To further resolve this question will probably require additional crystal structure analyses for other members of the deGFP family, crystal equilibration studies,[2] single-crystal absorption experiments, and perhaps further mutagenesis to dissect the individual contributions of key amino acids.

Structural Basis for Dual Emission. The strong blue fluorescence observed with deGFPs at low pH for excitation at 400 nm was initially surprising. We first conjectured that the blue fluorescence would be explained by a pH-dependent rearrangement of a preexisting proton relay, such as that described for wild-type GFP (*23*, *24*), preventing ESPT. The spectroscopy and structure analysis reported here, combined with the ultrafast excited-state measurements described in the companion paper (*42*), support this general notion. In this proposal, the neutral form of the excited chromophore is unable to undergo rapid proton transfer at low pH and emits at about 460 nm. At high pH, structural rearrangements result in an environment conducive to the discharge of a proton from the excited state of the neutral chromophore to a nearby acceptor. Subsequently, emission at about 515 nm from the excited state of the anionic chromophore is observed. Strong support for the predominance of ESPT in the mechanism of green fluorescence is provided by the excited-state dynamics and deuterium isotope effect observed in the companion paper (*42*). The rate of ESPT in deGFP is observed to slow either upon acidification or by subsitution of exchangeable protons with deuterium. These ESPT rates are generally slower than that observed in wild-type GFP (*21*), suggesting that the proton relay network in deGFPs is less efficient or geometrically optimal than that found in wild type.

In deGFPs it appears that a novel proton relay, not previously seen in crystal structures of any GFP variant, can support ESPT. The proton relay appears to consist of Ser147 and two water molecules (red dashed lines and atoms in Figure 3) and permits rapid proton transfer between the chromophore hydroxyl and the bulk solvent at high pH. Rearrangement of this network and removal of Ser147 from contact with the chromophore eliminate the proton relay at low pH. Model building experiments (see Figure 4) suggest that similar rearrangements, resulting in similar hydrogen-bonding networks, can take place in deGFPs 2−4 without severe steric clashes. We propose that the dual emission characteristics of all deGFPs can be described by this model.

[2] Elsliger et al. (*29*) carefully examined pH-dependent structural changes in S65T GFP and showed that the crystals could be equilibrated with mother liquor at either pH. Thus, conformational changes are not a consequence of differing crystal environments. In S65T the chain segment containing His148 undergoes small rearrangements in response to the protonation state of the chromophore hydroxyl; however, the backbone rearrangements seen in deGFP1 are an order of magnitude larger.

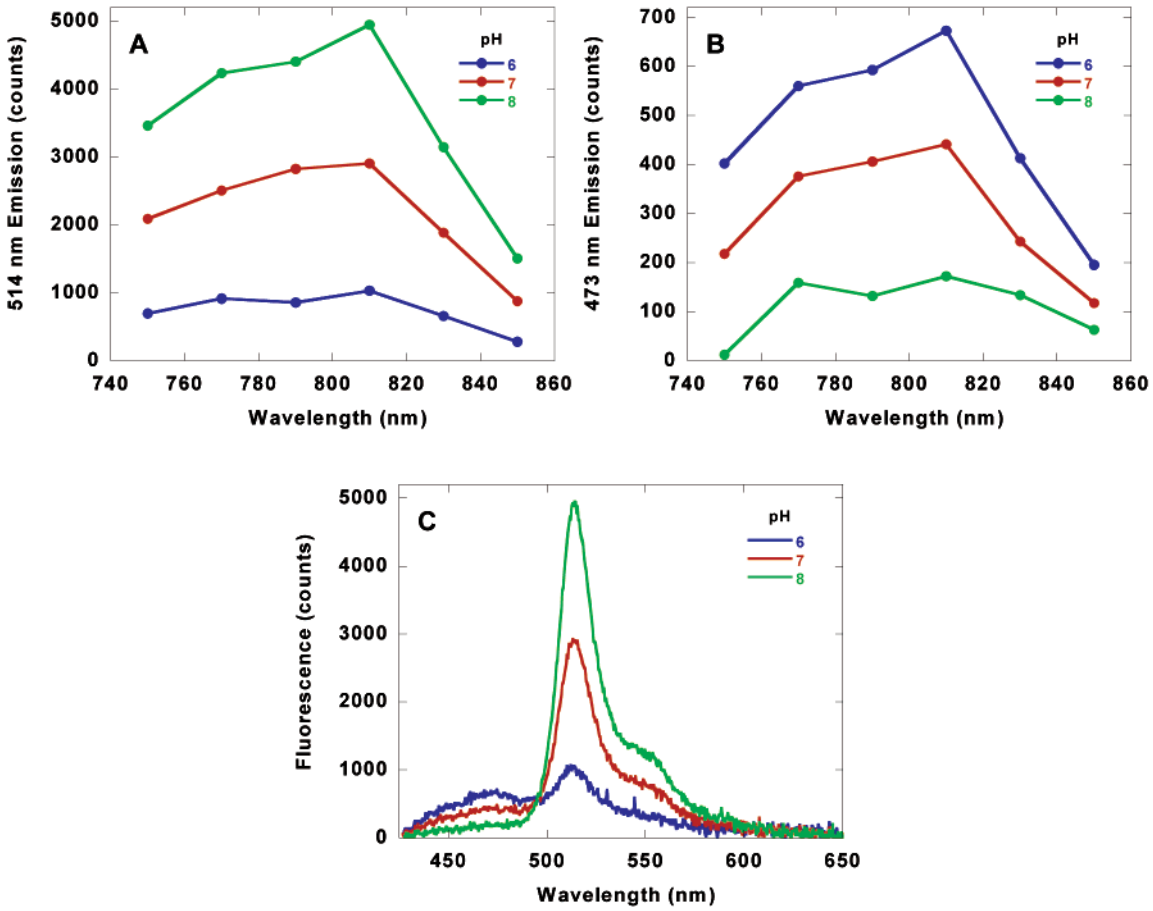

FIGURE 8: Fluorescence emission intensity as a function of two-photon excitation wavelength and pH. As described in Materials and Methods, light from a Ti:S laser excited droplets of purified deGFP4 (100 μg/mL) on the stage of a two-photon microscope, and emission was collected at an imaging spectrograph to quantify fluorescence at specific wavelengths. Results are presented as deGFP4 fluorescence counts above background. deGFP4 was dissolved in physiologic saline solution with pH adjusted to 6, 7, or 8. In response to indicated excitation wavelengths, fluorescence emission was quantified separately at (A) 514 nm and (B) 473 nm. At both emission wavelengths, peak excitation was observed near 810 nm. In response to a fixed 810 nm excitation (C), the deGFP4 fluorescence emission spectrum from 425 to 620 nm demonstrated similar pH sensitivity as in response to conventional excitation.

Comparison of the mutants presented in Tables 1 and 2 suggests that the cause of dual emission cannot be linked to a specific set of mutation sites since mutants with single cysteine substitutions at either residue 148 or 203 display dual emission. Thus, dual emission may be common in GFP variants. The substitution S65T is probably required to prevent Glu222 from being anionic and a proton acceptor in ESPT. The substitution of cysteine for polar residues has at least two different consequences: an increase in the hydrophobicity of the chromophore environment and a reduction in specific hydrogen-bonding capability associated with the chromophore hydroxyl group. To generalize these observations, dual emission behavior requires that the rate of ESPT be slow enough that emission can occur, at least to some extent, from the excited state of the neutral chromophore before deprotonation. ESPT, in turn, depends on the presence of a proton-transfer pathway from the chromophore to a suitable acceptor, and the rate of ESPT appears to depend on the specific nature of this pathway. For a detailed discussion of these relative rates, the reader is referred to the companion paper (*42*).

Wild-type GFP and deGFPs appear to have different proton-transfer pathways; thus the existence of ESPT pathways is exquisitely sensitive to the details of the protein structure. With this guiding principle in mind one might conceivably construct dual emission biosensors that would respond, by changes in ESPT pathways, to a variety of different cellular phenomena such as changes in ionic strength, redox potential, or specific binding events.

Application: Dynamic Response of deGFP4 in Vivo. To evaluate the suitability of deGFP4 for studies in mammalian cells, the protein was expressed in fibroblasts and imaged using both confocal and two-photon microscopy. Using UV confocal microscopy, cells expressing deGFP4 were shown to exhibit cytoplasmic fluorescence (Figure 5A,B). Fluorescence at 385−470 nm was only marginally above cellular autofluorescence; however, it is important to note that the experimental excitation wavelength of 364 nm is significantly different from the deGFP4's optimal excitation wavelength of 400 nm. The same cells were loaded with the ratiometric, pH-sensitive dye, SNARF-1 (Figure 5 C,D) and excited at 543 nm for direct comparison between the two pH indicators. Comparison of the signals from the four channels monitored before and after the cells were loaded with SNARF-1 reveals that there is very little overlap in the signals from deGFP4 and SNARF-1 (data not shown). A time−course experiment was carried out, and emission ratio changes were simultaneously monitored with deGFP4 and SNARF-1 in the same cells. Intracellular pH changes were imposed by transient exposure to 25 mM NH_4Cl. Due to rapid NH_3 transport and

NH_3/NH_4^+ equilibration, the cell cytosol promptly alkalinizes upon NH_4Cl addition to the continuous perfusion system and acidifies upon NH_4Cl removal (*43*). From the normalized trace obtained with each probe (Figure 6A) it is evident that deGFP4 has a greater dynamic range of ratio change than SNARF-1 over the tested pH range. However, results from deGFP4 are noisy because of the weak deGFP4 signal detected in the blue (385−475 nm) channel. As shown in Figure 6B, the total 385−470 nm fluorescence from deGFP4 expressing cells was clearly pH-sensitive but was only slightly greater than the fluorescence of untransfected cells in the same field of view. Conversely, Figure 6C shows that 475−525 nm fluorescence was much greater than background autofluorescence and responded to pH changes with qualitatively opposite changes in fluorescence versus the 385−470 nm emission range. Thus results from intracellular deGFP4 conform to expectations from the known spectral characteristics of purified deGFP4.

Although a detectable signal was obtained from conventional confocal microscopy, two-photon excitation microscopy provides a superior signal over background levels at the lower wavelength emission. Figure 7 shows images of PS120 cells transiently transfected with deGFP4 imaged in response to two-photon excitation at 810 nm. The blue emission peak from cells expressing deGFP4 is readily distinguished from the surrounding untransfected cells (compare Figure 7A to Figure 5A). The improved signal over background could be due to decreased cellular autofluorescence and/or more efficient excitation of the protonated deGFP4 in response to the 810 nm excitation.

Given the improvement from two-photon imaging, it was important to characterize the optimum excitation wavelength for two-photon excitation and to confirm the pH sensitivity of two-photon deGFP4 fluorescence. As shown in Figure 8A,B, 810 nm was the optimum excitation for two-photon fluorescence of deGFP4 over a range of pH values, for both the 473 and 514 nm emission peaks of deGFP4 fluorescence. A similar peak excitation value was reported for wild-type GFP (*44*) and might be anticipated from the observed peak of one-photon excitation of deGFP4 at ∼400 nm. The collection of two-photon fluorescence emission spectra from purified deGFP4 confirmed that the two-photon fluorescence retained the same pH sensitivity as reported earlier (shown in Figure 8C).

REFERENCES

1. Tsien, R. Y. (1998) *Annu. Rev. Biochem. 67*, 509−544.
2. Remington, S. J. (2000) *Methods Enzymol. 305*, 195−211.
3. Zimmer, M. (2002) *Chem. Rev. 102*, 759−781.
4. Wachter, R., King, B. A., Heim, R., Kallio, K., Tsien, R. Y., Boxer, S. G. Remington, S. J. (1997) *Biochemistry 36*, 9759−9765.
5. Kneen, M., Farinas, J. F., and Verkman, A. S. (1998) *Biophys. J. 74*, 1591−1599.
6. Llopis, J., McCaffery, J. M., Miyawaki, A., Farquhar, M., and Tsien, R. Y. (1998) *Proc. Natl. Acad. Sci. U.S.A. 95*, 6803−6808.
7. Miesenboeck, G., De Angelis, D. A., and Rothman, J. E. (1998) *Nature 394*, 192−195.
8. Sankaranarayanan, S., De Angelis, D., Rothman, J. E., and Ryan, T. A. (2000) *Biophys. J. 79*, 2199−2208.
9. Miyawaki, A., Llopis, J., Heim, R., McCaffery, J. M., Adams, J. A., Ikura, M., and Tsien, R. Y. (1997) *Nature 388*, 882−887.
10. Miyawaki, A., Griesbeck, O., Heim, R., and Tsien, R. Y. (1999) *Proc. Natl. Acad. Sci. U.S.A. 96*, 2135−2140.
11. Nagai, T., Sawano, A., Park, E. S., and Miyawaki, A. (2001) *Proc. Natl. Acad. Sci. U.S.A. 98*, 3197−3202.
12. Romoser, V. A., Hinkle, P. M., and Persechini, A. (1997) *J. Biol. Chem. 272*, 13270−13274.
13. Persechini, A., Lynch, J. A., and Romoser, V. A. (1997) *Cell Calcium 22*, 209−216.
14. Wachter, R. M., and Remington, S. J. (1999) *Curr. Biol. 9*, R628−R629.
15. Jayaraman, S., Haggie, P., Wachter, R. M., Remington, S. J., and Verkman, A. S. (2000) *J. Biol. Chem. 275*, 6047−6050.
16. Zacharias, D. A., Violin, J. D., Newton, A. C., and Tsien, R. Y. (2002) *Science 296*, 913−916.
17. Ting, A. Y., Kain, K. H., Klemke, R. L., and Tsien, R. Y. (2001) *Proc. Natl. Acad. Sci. U.S.A. 98*, 15003−15008.
18. Ostergaard, H., Henriksen, A., Hansen, F. G., and Winther, J. R. (2001) *EMBO J. 20*, 5853−5862.
19. Grynkiewicz, G., Martin, P., and Tsien, R. Y. (1985) *J. Biol. Chem. 260*, 3440−3450.
20. Heikal, A. A., Hess, S. T., and Webb, W. W. (2001) *Chem. Phys. 274*, 37−55.
21. Chattoraj, M., King, B. A., Bublitz, G. U., and Boxer, S. G. (1996) *Proc. Natl. Acad. Sci. U.S.A. 93*, 8362−8367.
22. Lossau, H., Kummer, A., Heinecke, R., Poellinger-Dammer, F., Kompa, C., Bieser, G., Jonsson, T., Silva, C. M., Yang, M. M., Youvan, D. C., and Michel-Beyerle, M. E. (1996) *Chem. Phys. 213*, 1−16.
23. Brejc, K., Sixma, T. K., Kitts, P. A., Kain, S. R., Tsien, R. Y., Ormo, M., and Remington, S. J. (1997) *Proc. Natl. Acad. Sci. U.S.A. 94*, 2306−2311.
24. Palm, G. J., Zdanov, A., Gaitanaris, G. A., Stauber, R., Pavlakis, G. N., and Wlodawer, A. (1997) *Nat. Struct. Biol. 4*, 361−365.
25. Yang, F., Moss, L. G., and Phillips, G. N. J. (1996) *Nat. Biotechnol. 14*, 1246−1251.
26. Ehrig, T., O'Kane, D. J., and Prendergast, F. G. (1995) *FEBS Lett. 367*, 163−166.
27. Heim, R., Prasher, D. C., and Tsien, R. Y. (1994) *Proc. Natl. Acad. Sci. U.S.A. 91*, 12501−12504.
28. Ward, W. W., Prentice, H. J., Roth, A. F., Cody, C. W., and Reeves, S. C. (1982) *Photochem. Photobiol. 35*, 803−808.
29. Elsliger, M.-A., Wachter, R. M., Hanson, G. T., Kallio, K., and Remington, S. J. (1999) *Biochemistry 38*, 5296−5301.
30. Robey, R. B., Ruiz, O., Santos, A. V. P., Ma, J., Kear, F., Wang, L.-J., Li, C.-J., Bernardo, A. A., and Arruda, J. A. L. (1998) *Biochemistry 37*, 9894−9901.
31. Terskikh, A., Fradkov, A. F., Ermakova, G., Zaraisky, A. G., Tan, P., Kajava, A. V., Zhao, X., Ding, L., Lukyanov, S. A., Matz, M. V., Kim, S., Weissman, I., and Siebert, P. (2000) *Science 290*, 1478−1479.
32. Matz, M. V., Arkady, F. F., Labas, Y. A., Savitsky, A. P., Zaraisky, A. G., Markelov, M. L., and Lukyanov, S. A. (1999) *Nat. Biotechnol. 17*, 969−973.
33. Awaji, T., Hirasawa, A., Shirakawa, H., Tsujimoto, G., and Miyazaki, S. (2001) *Biochem. Biophys. Res Commun. 289*, 457−462.
34. Gill, S. C., and von Hippel, P. H. (1989) *Anal. Biochem. 182*, 319−326.
35. Weber, G., and Teale, F. W. J. (1957) *Trans. Faraday Soc. 53*, 646−655.
36. CCP4 (1994) *Acta Crystallogr., Sect. D 50*, 760−763.
37. Tronrud, D. E., Ten Eyck, L. F., and Matthews, B. W. (1987) *Acta Crystallogr. A43*, 489−503.
38. Jones, T. A., Zou, J.-Y., Cowan, S. W., and Kjeldgaard, M. (1991) *Acta Crystallogr. A47*, 110.
39. Heim, R., and Tsien, R. Y. (1996) *Curr. Biol. 6*, 178−182.
40. Patterson, G. H., and Lippincott-Schwartz, J. (2002) *Science 297*, 1873−1877.
41. Ormo, M., Cubitt, A. B., Kallio, K., Gross, L. A., Tsien, R. Y., and Remington, S. J. (1996) *Science 273*, 1392−1395.
42. McAnaney, T. B., Park, E. S., Hanson, G. T., Remington, S. J., and Boxer, S. G. (2002) *Biochemistry 41*, 15489−15494.
43. Roos, A., and Boron, W. F. (1981) *Physiol. Rev. 61*, 296−434.
44. Niswender, K. D., Blackman, S. M., Rohde, L., Magnuson, M. A., and D. W. (1995) *J. Microsc. 180*, 109−116.
45. Kraulis, P. J. (1991) *J. Appl. Crystallogr. 24*, 946−950.

BI026609P